lubricants

MDPI

Review

Turbulence Effects in Tilting Pad Journal Bearings: A Review

Alberto Betti, Paola Forte and Enrico Ciulli *

Department of Civil and Industrial Engineering, University of Pisa, 56122 Pisa, Italy; alberto.betti@phd.unipi.it (A.B.); paola.forte@unipi.it (P.F.)
* Correspondence: enrico.ciulli@unipi.it

Abstract: This paper reviews the current knowledge on turbulence effects in tilting pad journal bearings. Turbulence is becoming increasingly important in the design of hydrodynamic bearings due to the trend to increase power density in turbomachines and consequently the operating speeds of the hydrodynamic bearings. Turbulence has a series of effects on the bearing performance which may be beneficial or detrimental, depending on the operating conditions. The main turbulence models are recalled and a historical overview on the evolution of numerical simulations of turbulent flow in tilting pad journal bearings is presented. The two broad simulation strategies used are the generalized Reynolds equation and computational fluid dynamics. The main experimental works are then reviewed, and a unified comparison of these works is provided. Novel results on the critical Reynolds number in a tilting pad journal bearing are reported. Much emphasis is given on the experimental evidence for laminar-to-turbulent transition. The evidence used in the literature is reviewed and its reliability is discussed. Lastly, some future research directions are suggested.

Keywords: tilting pad journal bearing; turbulence; Reynolds number; computational fluid dynamics; laminar-to-turbulent transition; experimental testing

check for updates

Citation: Betti, A.; Forte, P.; Ciulli, E. Turbulence Effects in Tilting Pad Journal Bearings: A Review. *Lubricants* **2022**, *10*, 171. https://doi.org/10.3390/lubricants10080171

Received: 17 June 2022
Accepted: 22 July 2022
Published: 26 July 2022

Publisher's Note: MDPI stays neutral with regard to jurisdictional claims in published maps and institutional affiliations.

1. Introduction

Hydrodynamic journal bearings can have a fixed or variable geometry. Their geometry can be controlled actively or passively [1]. Tilting pad journal bearings (TPJB) are amongst the most used passive variable geometry devices (Figure 1). The theoretical benefit of TPJBs is the well-known negligibility of cross-coupled dynamic coefficients, which are a source of rotor instability [2]. Moreover, they can tolerate some degree of manufacturing error [3] and misalignment [2].

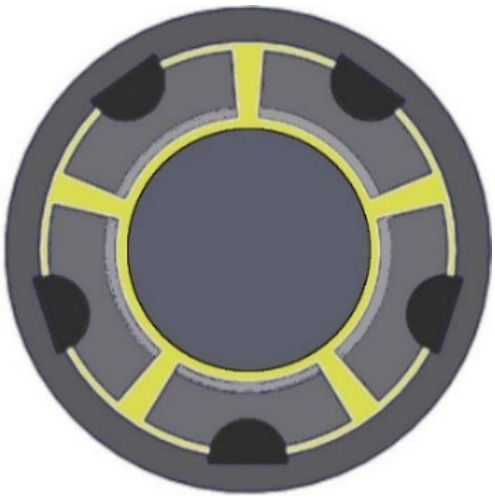

Figure 1. Schematic section of a 5-pad TPJB.

Hydrodynamic TPJBs are widely employed in large turbomachines for energy production, including nuclear power plants, or in standalone systems such as gear boxes, pumps, turbines, and compressors. The current trend in turbomachines for energy production is to convey increasingly higher power densities. This requirement opens design challenges in many components of the power plant, including the bearings. In principle, a higher power density can be achieved by rising the shaft angular speed. Higher rotor angular speed or larger bearing size means higher peripheral speed and a higher average circumferential Reynolds number, defined as:

$$Re_c = \frac{D}{2}\frac{\Omega C}{\nu} \tag{1}$$

where D is the bearing diameter, Ω is the shaft angular speed, C is the assembled radial clearance, and ν is the kinematic viscosity of the lubricant. At high speed, when Re_c exceeds a critical value (typically 1000 for oil-lubricated journal bearings [4]), the flow regime is expected to transition from laminar to turbulent flow. Commonly, the circumferential average Reynolds number Re_c is used in experiments to discern between laminar and turbulent flow regimes. However, a local Reynolds number Re_h, based on the local properties of the flow and independent of global features, is also defined. The local Reynolds number is often used in numerical simulations. Due to their different definitions, Re_c and Re_h have different critical values and cannot be used interchangeably. In bearings for turbomachines, Szeri [5] suggested a critical value in the range of $400 < Re_h < 900$ for the laminar-to-turbulent transition (LTT).

Fully turbulent flow is characterized by random fluctuations of its velocity and pressure fields. Moreover, it is three-dimensional, and it contains eddies in a large span of length scales. The presence of vortices increases energy dissipation with respect to the laminar case. A peculiar turbulent flow, typical of hydrodynamic bearings, is the Taylor vortices flow. It has been observed first by Taylor in rotating concentric cylinders [6]. This flow is characterized by macroscopic eddies, whose length scale is C. However, microscopically, the flow is still laminar. It is often difficult to assess whether turbulent flow in bearings occurs in the form of full turbulence or Taylor vortices, given that both, and even a combination of the two, have been observed [7]. Thus, some authors refer to turbulent flow, independent of its morphology [8–10]. Taylor vortices are expected to occur above a critical Reynolds number, given by the following criterion:

$$Re_{Ta} = 41.2\sqrt{\frac{D}{2C}} \tag{2}$$

Equation (2) strictly holds for plain, concentric cylinders. It has been shown that eccentricity between cylinders tends to delay the occurrence of Taylor vortices [11].

Some review articles on turbulence effects on bearing performance date back to a few decades ago. Taylor [4] reviewed classical turbulent lubrication theories, applied to the design of fluid film bearings. Wilcock [7] reviewed the findings presented at the Second Leeds-Lyon Symposium (1975), centered on experimental and numerical analysis of turbulent flow in bearings, with special attention to the transition range from laminar to turbulent conditions. Macken and Saibel [10] surveyed experimental and theoretical works on turbulence and inertia effects in different types of bearings, operating at high-speed or with unconventional lubricants. Since then, physical phenomena related to turbulence have been considered when simulating or testing a bearing. However, to the best of the authors' knowledge, there has been no recent in-depth review of the latest literature focused on TPJBs. In the following section, the main theoretical models of turbulent flow for fluid lubrication are recalled and the literature on numerical investigations on turbulent TPJBs is reviewed. Moreover, in the subsequent section, experimental works are reviewed, while in the final section, conclusions are presented along with some future research objectives.

2. Numerical Investigations

2.1. Turbulence Models

A classical way to model turbulent flow in thin films is to consider it as an extension of the laminar Reynolds equation by including the turbulent coefficients k_x and k_z:

$$\frac{\partial}{\partial x}\left(\frac{h^3}{k_x \mu}\frac{\partial p}{\partial x}\right) + \frac{\partial}{\partial z}\left(\frac{h^3}{k_z \mu}\frac{\partial p}{\partial z}\right) = \frac{U}{2}\frac{\partial h}{\partial x} \tag{3}$$

Equation (3) is one of the classical forms of the turbulent Reynolds equation in Cartesian coordinates, where x is the direction along which the lubricant is entrained by the solid surface in motion with the speed U, z is the direction of the lateral flow, y (not appearing in the formula) is the direction of the film thickness h, μ is the dynamic viscosity, and p is the pressure. It may be somewhat surprising that a complex phenomenon such as turbulence can be successfully included with a minimal modification of the laminar Reynolds equation. This can be justified by the concept of eddy viscosity, first introduced by Boussinesq [12]. Adopting this hypothesis, it was shown that the presence of turbulence can be described with an anisotropic, non-homogeneous effective viscosity, also referred to as turbulent viscosity. The turbulent viscosity value is a function of the local Reynolds number. The turbulent coefficients k_x and k_z monotonically increase as functions of the Reynolds number, starting from the laminar value of 12. When hydrodynamic lubrication theories were first developed, the lubricant was assumed isothermal for simplicity. In later works, the energy equation was also considered. In the same spirit of the Reynolds equation, turbulence was included in the energy equation by considering an anisotropic, non-homogeneous effective conductivity of the lubricant. This effective conductivity is not a physical property of the fluid. Instead, it is a simplified description of heat transfer which accounts for vortices convection in a thin film. The effective conductivity value is a function of the local Reynolds number, amongst other variables (see, for instance, [13]).

Different theories have been proposed to calculate the expression for the turbulent coefficients. Some explicit expressions can be found, for instance, in Taylor [4]. The classical theories were not derived from first principles—they are based on some degree of empirical information. Such theories obtain slightly different expression for k_x, k_z depending on which empirical information is exploited and depending on the assumptions utilized in the derivation. Costantinescu [13,14] obtained the turbulent Reynolds equation using Prandtl's mixing length theory [15]. Ng and Pan [16] developed a linearized model based on Reichardt's formula assuming a shear dominated film. Elrod and Ng [17] extended Ng and Pan's linear theory including pressure gradient effects. They proposed a non-linear turbulent Reynolds equation for which iterative calculations are required to solve the problem. An empirical drag law relating the wall shear stresses and the mean flow velocities was proposed in the bulk flow theory of Hirs [18]. Ho and Vohr [19] employed a kinetic energy approach using Kolmogorov's turbulence theory. Aoki and Harada [20] utilized Prandtl's mixing length theory including pressure gradients and centrifugal effects. Hashimoto and Wada [21] extended Hirs' bulk flow theory including surface roughness effects. Tieu and Kosasih [22] used Prandtl's mixing length theory and extended it by considering the effect of shear stress gradient on the mixing length.

In Figure 2, values of the turbulent coefficients as functions of the Reynolds number are reported for a selection of theories. These theories stood the test of time and are successfully employed in commercial software which solves the generalized Reynolds equation together with the energy equation.

Some studies [19,23,24] have compared a selection of the above theories and have concluded that they give generally similar, satisfactory results in typical, oil-lubricated bearing applications, albeit some disagreement between theories can be found near the LTT region. Nevertheless, for low-viscosity, highly turbulent films, such as water or gas lubricated bearings, computational fluid dynamics (CFD) is required, also due to a shortage of experimental data [25].

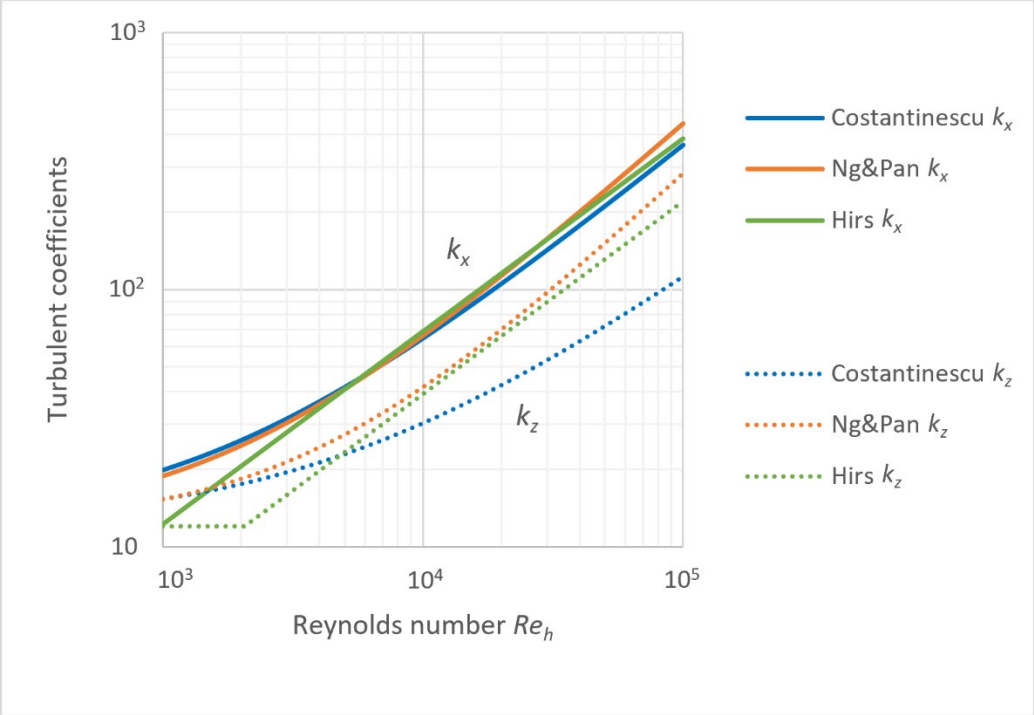

Figure 2. Turbulent coefficients as functions of the local Reynolds number according to Costantinescu [14], Ng and Pan [16], and Hirs [18] turbulent lubrication theories. Continuous and dashed lines indicate, respectively, values of k_x and k_z.

Currently, numerous turbulent models have been implemented in CFD simulations of TPJBs, with different complexity. They are reviewed and compared in Ding et al. [26]. Most of them employ Boussinesq's hypothesis and are employed within the Reynolds-averaged Navier-Stokes (RANS) framework. Listed in order of increasing complexity: the Spalart-Allmaras model [27] is based on one additional equation for the kinematic eddy turbulent viscosity; the k-ε and k-ω models [28,29] use two additional partial differential equations for the turbulence kinetic energy and its dissipation rate; Menter's shear stress transport (SST) model [30] was developed as a combination of the k-ε and k-ω model. The above models are considered adequate to simulate TPJBs in industrial applications [31].

Some researchers have employed more advanced turbulent models in other types of hydrodynamic bearings, namely plain [32,33] or thrust pad bearings [34]. In the Reynolds stress equation model, the Boussinesq's hypothesis is dropped, and it is considered more suited to deal with complex flows. In the AKN k-ε model [35], separating and reattaching turbulent flows for low-Re can be modelled. The employability of these models depends on how mature they are since they can be tuned by varying multiple coefficients.

2.2. Numerical Analysis

In the literature, there are several strategies used to solve the turbulent lubrication problem of a TPJB. These have different degrees of complexity and computational cost. On the one hand, there are bearing codes that perform hydrodynamic (HL), thermo-hydrodynamic (THL), and thermo-elasto-hydrodynamic (TEHL) lubrication analysis based on the generalized Reynolds equation. On the other hand, there is CFD software for a full 3D solution of the Navier-Stokes equations, dropping the simplifying assumptions of the Reynolds equations. In both cases, turbulent modelling is included. The former cases provide faster and cheaper numerical solutions for the pad assembly, while the costlier CFD is usually devoted to validation purposes. Some authors have utilized both approaches and compared the results. Yang and Palazzolo [36] reviewed the development history of numerical simulations of TPJBs based on the generalized Reynolds equation and CFD.

Their review described the evolution of simulation features particularly regarding energy and elasticity. The present review is more limited in scope since it focuses on a selection of works on TPJBs which are related to turbulence effects. Table 1 summarizes the examined theoretical studies, highlighting the adopted turbulence models, the solution method, and the numerical grid for the hydrodynamic film. The works are listed in chronological order. Some articles reported the number of grid points across the three directions: radial (R), circumferential (θ), and axial (Z); others reported only the total number of grid points. Whenever a single number is indicated in the column for grid points, it refers to the total number of points. Next to the grid column, the geometry column specifies geometric dimensions relevant to the hydrodynamic film: the radial clearance (C), the pad arc length ($R\theta$), and the pad axial length (L). These quantities are reported in millimeters.

Most articles in Table 1 model four or five pad TPJB. Three pads are instead modelled in [37,38], and six pads in [39]. Most studies use ISO VG 32 oils. Others use a ISO VG 46 oil [37], silicon oils [40], water [25,41,42], and supercritical CO_2 [38]. Apart from a few exceptions, most numerical studies are validated by comparison with experimental results from the literature or obtained through their own experimental activity as reported by [37,39,40,43–49]. In the next subsections, some discussion on the articles listed in Table 1 is provided.

2.2.1. Studies Based on Generalized Reynolds Equations

Analytical approaches have been proposed to solve Equation (3) in TPJBs with the assumption of isothermal conditions and no deformation in [41,42]. Okabe and Cavalca [41] used the short bearing approximation. They compared two analytical models with and without a turbulence factor correction. They performed a rotordynamic simulation of a Jeffcott rotor supported by two TPJBs and concluded that turbulence increased the hydrodynamic forces and the stiffness coefficients. Jin and Yuan [42] compared the analytical results to those obtained through a finite difference method (FDM) solution. They observed that the effect of turbulence on the predicted journal orbits depended on the applied static load.

Other isothermal and no-deformation solutions of the Reynolds equation by FDM were presented in [25,45]. Armentrout et al. [25] used the Elrod and Ng turbulence model with a variable parameter within the empirical Reichardt's formula. They tuned the model parameter by comparing results with CFD. However, the optimal parameter ended up being geometry dependent.

The energy equation was added to the 2D Reynolds equation, removing the isothermal assumption, and without considering deformation, in [39,43,50–53]. In his pioneering work, Ettles [54] considered a 1D energy equation and a 1D elasticity equation. However, most of the other works exploit a 3D energy equation.

Table 1. Numerical works—turbulence modelling in TPJBs.

Authors	Lubricant	Model [1]	Turbulence Model	Method [1]	Grid [2] $R \times \theta \times Z$	Geometry [2] $C \times R\theta \times L$ (mm)	Experimental Verification
Orcutt, 1967 [40]	Silicon oil	HL	Ng & Pan	-	-	-	Yes
Mikami et al., 1988 [39]	ISO VG 32	THL	Aoki & Harada	-	-	-	Yes
Taniguchi et al., 1990 [43]	ISO VG 32	THL	Ng & Pan	FDM	9 × 9 × 9	0.612 × 334 × 300	Yes
Ettles, 1992 [54]	-	TEHL	T boundary conditions	-	-	-	Yes, data from [43,55–57]
Bouard et al., 1996 [23]	ISO VG 32	THL	Ng & Pan Elrod & Ng Costantinescu	FDM	101 × 21 × 11	0.612 × 334 × 300	Yes, data from [43]
Edney et al., 1998 [44]	Light turbine oil	CFD	k-ε	FVM	8500	0.127 × 71 × 95	Yes
Tanaka and Hatakenaka, 2004 [51]	ISO VG 32	THL	Aoki & Harada 3D Aoki & Harada Ng & Pan	FDM	100 × 8 × 8	0.612 × 334 × 300	Yes, data from [39,43]
Ikeda et al., 2006 [45]	ISO VG 32	HL	Aoki & Harada	FDM	-	-	Yes
Okabe and Cavalca, 2009 [41]	Water	HL	Costantinescu	Analytical	-	-	No
Hatakenaka, 2015 [52]	ISO VG 32	THL	k-ε low Re	FDM	100 × 32 × 20	0.612 × 334 × 300	Yes, data from [43]
Armentrout et al., 2017 [25]	Water and oil	HL	Elrod & Ng	-	10 × 40 × 10	0.152 × 213 × 381	No
		CFD	k-ε low Re	-	17 × 200 × 175		
Ding et al., 2018 [26]	ISO VG 32	CFD	14 different models	-	50 × 100 × 20	0.612 × 334 × 300	Yes, data from [43]
Croné et al., 2018 [58]	ISO VG 32	CFD	SST	FEM moving mesh	13 × 161 × 19	0.32 × 314 × 350	No
Hagemann and Schwarze, 2018 [47]	ISO VG 32	TEHL	Costantinescu	FVM	-	-	Yes
		CFD	-	-	820,000	0.108 × 73 × 72	
Mermertas et al., 2019 [37]	ISO VG 46	TEHL	Costantinescu	FEM coupled FVM	-	-	Yes
Arihara et al., 2019 [46]	ISO VG 32	TEHL	Elrod & Ng	FDM	101 × 38 × 22	0.162 × 64 × 76	Yes
Jin and Yuan, 2020 [42]	Water and oil	HL	Ng & Pan	Analytical	-	0.152 × 213 × 381	Yes, data from [25,59]
				FDM	1 × 21 × 15		
Hagemann et al., 2020 [48]	ISO VG 32	TEHL	Costantinescu	-	-	-	Yes
Yang and Palazzolo, 2021 [36]	ISO VG 32	TEHL	-	-	-	-	Yes, data from [60,61]
		CFD, elasticity	SST with γ transition model	FEM coupled FVM	-	-	
Buchhorn et al., 2021 [49]	ISO VG 32	TEHL	-	FEM	-	-	Yes
		CFD	SST	FVM	-	-	
Bi et al., 2021 [38]	S-CO_2 and oil	Compressible THL	Ng & Pan	FDM	1 × 32 × 26	0.01 × 41 × 40	Yes, data from [62]

[1] HL: hydrodynamic lubrication. THL: thermo-hydrodynamic lubrication. TEHL: thermo-elasto-hydrodynamic lubrication. CFD: computational fluid dynamics. FEM: finite element method. FDM: finite difference method. FVM: finite volumes method. [2] Hydrodynamic film characteristic.

3D TEHL models considering turbulence were developed in [46,48,49,63,64]. Thermal and mechanical deformations modify the film geometry. It is concluded that the elastic deformation can largely affect static and dynamic bearing performances. Mechanical deformation is often computed through commercial structural mechanics software, which solves the 3D elasticity equations by the finite element method (FEM). The elasticity equations are coupled to the thermo-hydrodynamic calculations. Yang [63] showed that the validity of both static and dynamic results depends on the choice of the mixing coefficients, which is often left to the analyst's experience. Their uncertainty can be decreased by employing CFD simulation of the flow between pads.

The total number of grid points used in HL, THL and TEHL simulations has not increased much throughout the last few decades. Some authors used a grid distribution

consistent with the domain geometry, so that the circumferential direction had more points than the radial and axial direction [25,26,58]. Others [41,46,51] followed the suggestion made by Bouard et al. [50], that the highest number of grid points should be adopted across the film thickness. Bouard and coworkers achieved convergence with 101 points across the radial direction for a turbulent flow. In contrast, only 38 points across the radial direction were required for a laminar flow.

In summary, it seems that 10^5 points in the hydrodynamic film are enough for state-of-the-art turbulent TEHL or THL simulations of TPJBs for a wide range of bearing geometric dimensions, and that this number can likely be reduced by 1 or 2 orders of magnitudes for the turbulent HL simulations. However, there is still some debate on the most effective grid point distribution. If the number of points across the film thickness is much lower than 100, extra attention to the convergence of the solution is recommended.

2.2.2. Studies Based on the CFD Simulations

One of the first applications of CFD to the analysis of a TPJB is found in Edney et al. [44]. Here, the effect of a profiled, leading edge groove (LEG) on the pad and its modification were investigated. The analysis was 2D and it was used to optimize the bearing design. It provided a detailed visualization of the thermal behaviour that could not be obtained with a common bearing analysis code. More recently, Croné et al. [58] have investigated the effect of a LEG TPJB by CFD analysis. They compared the LEG TPJB with a conventional one. The LEG pad yielded a higher maximum pad surface temperature due to a more pronounced transition from turbulent to laminar flow near the trailing edge.

The CFD simulations are useful to tune the computationally economical Reynolds model. The tuning can involve mesh refinements or the adjustment of turbulence model parameters [25]. Moreover, it can involve the calculation of thermal boundary conditions through an accurate determination of the heat flow [49]. In fact, the CFD solution is considered a good benchmark, despite some inherent uncertainties due to modelling assumptions and discretization errors. The main drawback is the time needed to setup and to run an analysis. Regarding turbulence models adopted in CFD analysis of TPJBs, Ding et al. [26] compared several turbulence models with experimental results from Taniguchi et al. [43]. They concluded that the SST model with low-Re correction outperforms all the others in replicating the experimental results.

Some authors commented on the ratio of turbulent to dynamic viscosity obtained through CFD simulations. Figure 3 was generated using data from [26,58].

The datasets in Figure 3 were taken from the numerical simulation of a conventional pad, on the pad center line. Both simulations employed the SST turbulence model. The simulations had different geometries and boundary conditions. Nevertheless, in Figure 3 it appears that turbulence has a maximum near the leading edge and has lower values towards the trailing edge. From the bearing pad designer's perspective, turbulence is desirable mainly at the trailing edge, where the pad temperature is highest, and it is unwanted elsewhere. This opens the question as to whether it is possible to realize a trend opposite to the one depicted in Figure 3, which would require reducing turbulence at the inlet and increasing it at the outlet. In addition, Ding et al. [26] compared the turbulent to dynamic viscosity ratio obtained with different turbulence models, showing a great variability amongst the models. Croné et al. [58] compared the conventional tilting pad to a LEG pad. They observed that the LEG mainly affected the region near the inlet. In particular, the maximum turbulent to dynamic viscosity ratio decreased in the center line and increased towards the axial edges.

The first TPJB model including 3D-CFD with multiphase flow, thermal-fluid interaction, turbulence transition, convective term in the energy equation due to shaft spin, pivot flexibility, and thermal mechanical distortions by two-way fluid-structure interaction modelling was presented in Yang et al. [63]. They concluded that the dynamic coefficients obtained by a conventional Reynolds approach with mixing coefficients were quite different compared to those obtained by CFD.

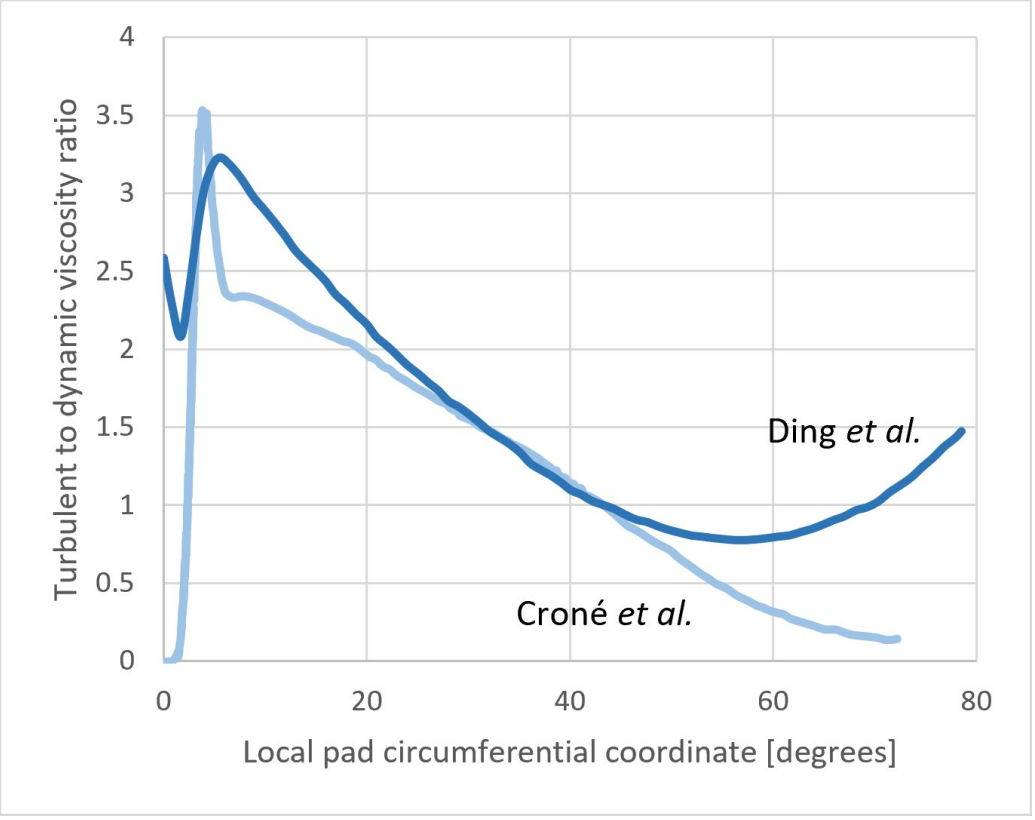

Figure 3. Turbulent to dynamic viscosity ratio on the pad center line, as a function of the local pad circumferential coordinate, for a conventional tilting pad (data from [26,58]).

The total number of grid points in CFD simulations has been increasing steadily throughout the years, and this trend is expected to continue, as more complex turbulence models will be developed. From Table 1, it appears that 10^6 points in the hydrodynamic film are enough for RANS CFD simulations of TPJBs for a wide range of bearing geometric dimensions.

2.3. Effect of Turbulence on the Bearing Performances

A feature which is unique to numerical works is the possibility to compare laminar and turbulent simulations. In experiments, the fluid is either laminar or turbulent. In simulations, instead, one can play with the different settings. The net effect of turbulence can then be assessed by comparing turbulent and laminar simulations. At low Reynolds, the laminar and turbulent theories are equivalent. At increasingly high Reynolds, the results from the two theories diverge [40]. It is considered good practice to check the results of turbulent simulation with the laminar simulation, given the lower computational cost of the latter [23].

In Figure 4, the typical profile of temperature as a function of the film thickness is reported. The figure is reproduced from [65]. In the turbulent simulation, the temperature gradient is reduced owing to an increase in the effective conductivity. This effect is beneficial to the pad temperature.

Compared to the laminar models, the turbulent models predict, above transition, an increase in load capacity [25,39,40] and power loss [23,39,40,52].

Fewer authors report the effect of turbulence on dynamic coefficients. Orcutt [40] and Okabe [41] found an increase in stiffness and damping coefficients. The magnitude of these effects is greatly dependent on the operating conditions.

Numerical models are currently capable of replicating typical experimental features associated to LTT, such as the drop in the pad maximum temperature [43,46,48,51,54,64]

and the increase in power loss [43,46,51,54]. These effects will be better explained and discussed in the following sections.

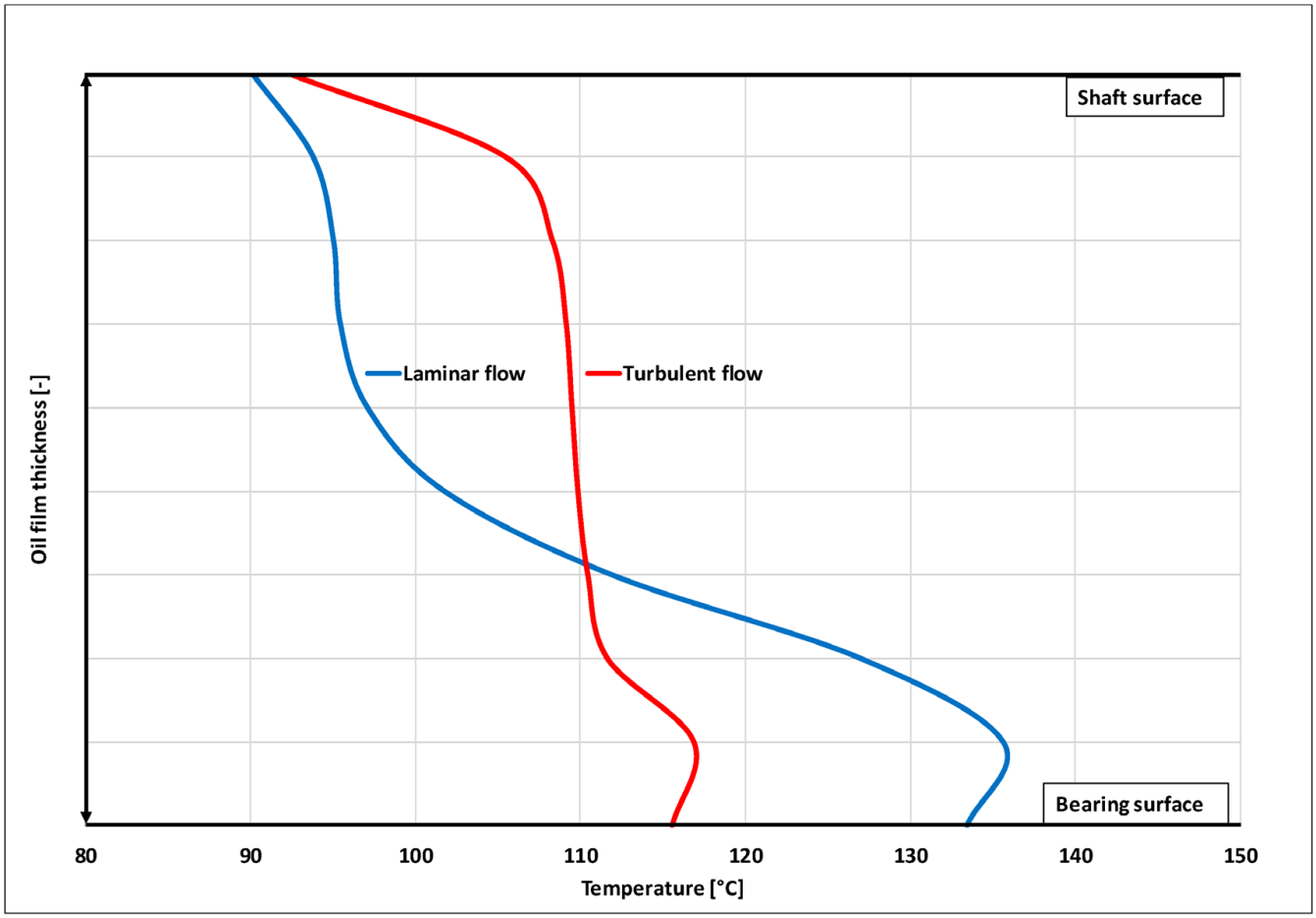

Figure 4. Typical temperature profile across the film thickness, in the laminar and turbulent regime. Reproduced from [65].

3. Experimental Works

3.1. Experimental Investigations with Turbulence

Not many works present evidence of LTT in experimental tests on TPJBs. A selection of recent papers is reported in this section, as well as some related fundamental ones. Some papers report, in addition, the results of tests performed with different types of bearings, such as plain journal bearings and fixed pad journal bearings. However, only TPJB data are reported here.

Table 2 summarizes the examined experimental studies of TPJBs in turbulent conditions. The bearing characteristics and the operating conditions are reported, as well as the evidence of the turbulent transition. Some data were directly extracted from the papers; other data were extrapolated and homogenized for easier comparison. For instance, papers usually report the operating speed in rpm, and the load in N. Here, instead, speed is reported as peripheral speed (m/s), and the load as specific load (MPa), which is load divided by nominal diameter and axial length. The works are reported mainly in chronological order, gathering together tests performed in the same test rigs.

Table 2. Experimental works—turbulence effects in TPJBs.

Authors	*D* (mm)	*L*/*D*	*C* (‰)	Max Speed (m/s)	Max Load (MPa)	Load Type [1]	Pads [1]	Lubrication Type [1]	Max Flow Rate (L/s)	Oil Supply *T* (°C)	Transition Evidence [2]	Re_c at Transition [3]
Gardner and Ulschmid, 1974 [55]	432	0.35	1.57	84	1.0	LOP	5	FL	2.2	43	PMT, PLI, ODT	670
De Choudhury and Masters, 1984 [56]	127	0.3	2.16	86	1.7	LOP and BP	5	FL	0.3	49	PMT	370
Mikami et al., 1988 [39]	150	1.33	2.6	24	1.47	LOP	6, RB	FL	-	60	-	300 *
Hopf and Schüler, 1989 [8]	500	0.9	1.35	94	4.0	LBP	4, B&S	-	-	40	PMT	820
Hagemann et al., 2013 [66] Kukla et al., 2013 [67]	500	0.7	1.28	79	2.5	LBP	5, EC	FL	7.0	50	-	1170 *
Buchhorn et al., 2021 [49]			1.2	79	3.0			DL	7.1	50	-	1100 *
Stottrop et al., 2022 [68]				79	4.0			FL and DL	7.1	50	SMT	860
Taniguchi et al., 1990 [43]	479	0.63	2.56	100	2.1	LBP	4	FL	8.7	40	PMT, PLI	950–1430
Simmons and Dixon, 1994 [69]	200	0.4	1.15 and 1.8	105	4.1	LOP and LBP	5, RB	FL	2.37	43	PMT, PLI, PITV	250–450
Ha and Kim, 1995 [70]	301	0.5	3.04	66	0.5	LBP	4, EC	FL	2.0	40	SMT	540–610
Edney, 1995 [71]	127	0.75	2.72–4.76	106	0.2	LBP	5, EC	FL	0.8	49	PMT, PLI	570–810
	102	0.5 0.75	2.99–4.58	86	0.5				1	49	PMT	580–650
Edney et al., 1998 [44]	127	0.75	1.85	120	0.2	LBP	5, EC	DL	0.5	49	-	630 *
Bouchoule et al., 1996 [72]	160	1.0	1.81 and 1.96	104	3.4	LBP	5, RB and B&S	DL	2.8	50	PMT	610
Ikeda et al., 2006 [45]	580	0.55	1.30	109	2.9	LBP	4, RB	DL	12.9	45	-	1580 *
Hagemann and Schwarze, 2018 [47]	120	0.60	1.80	94	2.0	LBP	4, RB	DL	0.7	50	PMT, PLI	290
Hagemann et al., 2020 [48]	100	0.9	2.6	140	4.0	LBP	5, RB	From FL to partially starved	1.3	40	PMT	280–410
Zemella et al., 2020 [64]				120	3.0							320
Arihara et al., 2019 [46]	102	0.75	3.19	120	2.9	LBP	4, FP	FL	1.7	40	PMT, SMT, PLI	370
Ferraro et al., 2020 [73] Ciulli et al., 2021 [74]	280	0.70	1.43–1.78	114	1.7	LBP	5, RB	DL	7.5	40–60	-	890 *–1880 *
	280	0.55	1.57–1.82	88	2.1			FL	3.6	40	PMT, PLI	470
	280	0.70	1.33–1.76	88	1.7		4, B&S	FL	2.7	40	PMT, PLI	450
Schüler and Berner, 2021 [65]	120	0.63	2.25	145	4.0	LBP	5, RB	DL	1.3	56	PMT	1050

[1] RB: rocker back (line contact), B&S: ball and socket (point contact), EC: elliptical contact, FP: flexural pivot; LOP: load on pad, LBP: load between pads; FL: flooded lubrication, DL: direct lubrication. [2] PMT: pad max temperature, SMT: shaft max temperature, PLI: power loss increase, ODT: oil discharge temperature, PITV: pad inlet temperature variance. [3] Reynolds calculated using oil supply temperature. * Reynolds calculated at bearing maximum speed.

In particular, the first column of the table references the examined work; the following columns report the main geometrical dimensions of the TPJB: the nominal diameter (D), the axial length to diameter ratio (L/D) and the per mille relative bearing clearance ($C‰$), which is the assembled radial clearance divided by the nominal radius, per mille. For each work, the investigated maximum peripheral speeds and specific loads are reported. Next, the load direction, which can be on pad (LOP) or between pads (LBP), is provided. In the pad column, the number and type of tilting pads, such as theoretical line contact, or rocker back (RB), and theoretical point contact, or ball and socket (B&S), are reported. In certain cases, the back of the pad is also axially curved; that is indicated, in the table, as elliptical contacts (EC). Then, information on the lubrication conditions is given: the maximum flow rate, the oil supply temperature, and the lubrication type, which can be flooded (FL), direct (DL), with leading edge grooves (LEG) or trailing edge grooves (TEG). In direct lubrication, the oil is directly supplied to the hydrodynamic film and it is free to leave the bearing—there is little to no secondary flow. In contrast, in flooded lubrication the pad is fully surrounded by oil. This can be achieved by confining the oil in the bearing with annular seals. The second-last column specifies the nature of the evidence for the LTT (see Section 3.2). The last column reports the circumferential average Reynolds number at transition, estimated through Equation (1).

Not all the papers in this table had measured or published experimental evidence for the LTT. However, these additional works were included due to their high Reynolds number at the highest operating speeds. In the cases lacking turbulence data, on the basis of reasonable considerations, the authors calculated the Reynolds number at the maximum operating speed, reporting it in the last column, and marking it with an asterisk. More details on the types of LTT evidence are deferred to Section 3.2 and the following ones. Some discussion on the calculation of the Reynolds number takes place in Section 3.5.

The tested bearings reported in Table 2 can be grouped by size with the smaller diameters ranging from 100 to 200 mm [39,44,46–48,56,64,65,69,71,72] and the larger ones from 280 to 580 mm [8,43,45,49,55,66–68,70,73,74]. The length to diameter ratio goes from a minimum of 0.3 [56] to a maximum of 1.33 [39]. The relative bearing clearance goes from a minimum of 1.15‰ for a diameter of 200 mm [69] to 4.76‰ for a diameter of 127 mm [71]. The maximum tested peripheral speed is 145 m/s [65], while the maximum tested specific load is 4.1 MPa [69]. Most bearings were tested in the LBP configuration with four or five pads. A six-pad bearing was tested by [39]. Most pads have a rocker back pivot, some have an elliptical contact pivot, some a ball and socket pivot, and one has a flexural pivot [46]. Most bearings are subjected to flooded lubrication; some are equipped with spray bars for direct lubrication. The maximum flow rate is 12.9 L/s, attained in [45] by direct lubrication. The oil supply temperature ranges from 40 to 60 °C.

Most papers in Table 2 employ test rigs with the floating bearing configuration, where loads are applied to the test bearing located at the shaft midspan. Two bearings were simultaneously tested in [56] loading the shaft at midspan. Two bearings were also tested in [71], three in [72], in particular facilities accommodating a steam turbine and gearboxes, respectively.

The experimental facility used by Hopf and Schüler [8], and other researchers after them [49,66,68], deserves particular mention for the high resolution of measurements of oil film thickness and pressures and shaft temperatures. The hollow shaft is equipped with two capacitive distance sensors, two piezoelectric pressure sensors and several thermocouples. Moreover, the rotating shaft can be axially shifted thanks to a special device. This allows for the mapping of quantities also along the axial direction, in addition to the circumferential direction. Pad temperatures are measured by means of 100 thermocouples located 5 mm below the sliding surface.

The work of Gardner and Ulschmid [55] is often cited in the following works. Temperatures were measured in several points of the Babbitt coating of the pads. Magnetic reluctance probes were placed at the leading and trailing edges of the loaded bottom pads in order to measure the film thickness. They monitored the power loss, the pad temperature,

and the oil discharge temperature. The friction coefficient was plotted as a function of the Reynolds number. They observed turbulence transition at about 2500 rpm.

The work of Taniguchi et al. [43] is another study used as a reference for following studies. There was a general agreement between experimental and numerical results obtained by turbulent models. The turbulent transition speed was observed between 2400 and 3000 rpm. They suggested that the situation of the unloaded pads plays an important role for the total friction losses: at 2400 rpm the loaded pads may still operate in the laminar regime, while the unloaded pads are already in the turbulent regime. Only at higher speeds (3000 rpm) do the loaded pads also enter into the turbulent regime.

3.2. Evidence for Turbulence Transition

The earliest experimental evidence for LTT was obtained by direct observation of turbulent flow in plain bearings. Wilcock [7] reviewed some papers on the morphology of turbulent flow in plain bearings. In these works, the flow pattern was visualized by dye injection, or by suspension of aluminum pigment particles. This method requires large clearances ($C‰ > 10$) which are usually not the case in industrial applications of TPJBs.

An alternative direct method to detect LTT requires the measurement of fluid velocity through anemometry techniques. The transition speed is detected by a sharp increase in the slope of the RMS velocity as a function of speed. Frêne and Godet [75] employed hot film wall anemometry to detect transition in a water lubricated plain bearing down to a 3‰ relative clearance. Innes and Leutheusser [76] employed hot wire anemometry in a large scale model of a thrust tilting pad in air. Tieu et al. [77] employed Laser Doppler Anemometry (LDA) in large-clearance ($C > 490$ μm), plain journal bearings lubricated by oil or water. They measured the velocity profile in the fluid at high Reynolds numbers up to 4700. They found excellent agreement with their turbulent model, described in [22]. More recently, Nobis et al. [78] applied LDA in an oil-lubricated plain bearing with $C‰ = 25$. In fact, with the evolution of the technique, it may be possible to apply LDA to smaller clearances. For a review on this technique, see, for instance [79].

Given the difficulty of applying direct methods in industrial TPJBs, a variety of indirect methods have been used in the literature to identify transition. Rather than measuring the fluid velocity itself, other macroscopic and easily measurable quantities are exploited. In the latter case, some degree of ambiguity is retained due to the indirect, albeit physically justified, evidence. A summary of the experimental methods is reported in Table 3.

Table 3. Main evidence used for laminar-to-turbulent transition in TPJBs.

Method	Evidence	Measured Quantity	References
Visual observation	Direct	Flow patterns	[7] *
Anemometry		Fluid velocity	[75–78] *
PMT	Indirect	Pad temperature	[8,43,46–48,55,56,65,69,71,72,74]
PLI		Power loss	[43,46,47,55,69,71,73]
SMT		Shaft temperature	[46,68,70]
ODT		Oil temperature	[55]
PITV	Speculative	Pad temperature	[69]
Journal shift		Journal position	[74]

* Not TPJBs.

One of the most utilized pieces of evidence is the reduction of the pad maximum temperature with increasing speed, on the loaded pads. For the sake of brevity, this method will be referred to in this work as PMT (pad maximum temperature). The point of maximum temperature in the loaded pad is near the trailing edge and it is monitored by a thermocouple placed at 75% of the circumferential length of the pad, in accordance with industry guidelines [80]. Figure 5 reports data from [69]. The pad maximum temperature is plotted as a function of speed. Different curves are taken at different loads.

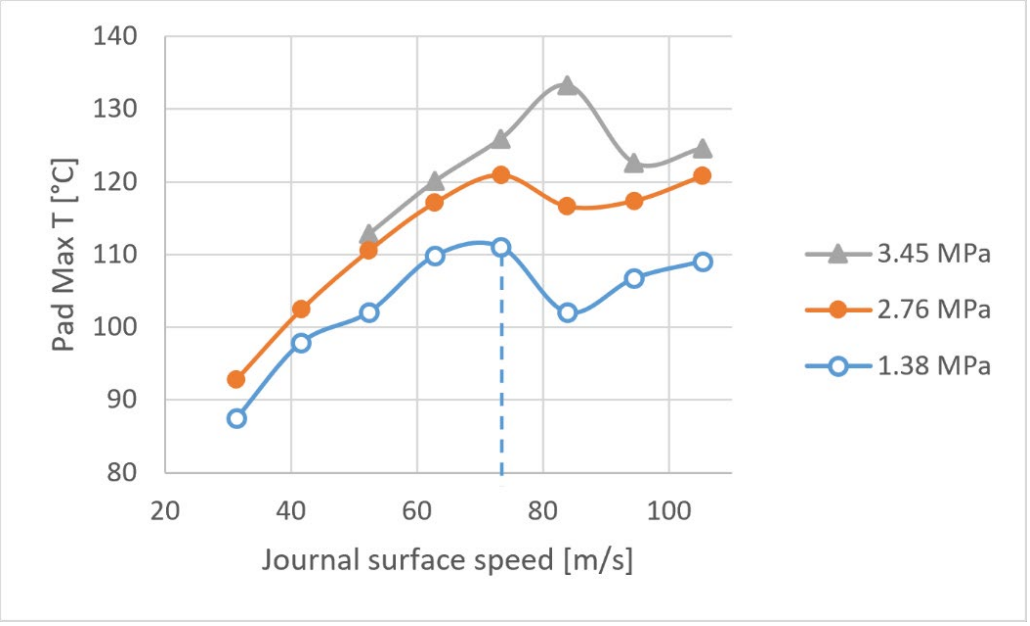

Figure 5. Pad maximum temperature as a function of journal surface speed. Curves are taken at different specific loads. The transition speed for the bottom curve is marked with a dashed line. Data from [69], configuration #1.

The onset of LTT is identified at the local maximum of the curves in Figure 5. As an example, the dashed line in Figure 5 is taken as the transition speed for the least loaded case (1.38 MPa). In this case, the transition speed is approximately 75 m/s. This effect is actually beneficial to the performance of the TPJB, since the maximum temperature of the pad is a quantity which it is always desirable to reduce. The magnitude of the temperature reduction may vary depending on the experimental conditions and can reach up to 10–15 K [8].

A similar effect is the reduction of the shaft temperature with increasing speed. This method will be referred to as SMT (shaft maximum temperature). This is less common to observe mainly because fewer authors measure or report data on the shaft temperature. Moreover, the shaft temperatures are typically lower than the maximum temperature of the loaded pads. One of the reasons is that a point on the pad sees the same film thickness in time, while a point on the shaft sees a variable film thickness along the bearing circumference. The temperature reduction (of the pad or the shaft) was seen as an odd phenomenon, since according to the laminar theory, temperature should always increase with speed. The origin of the temperature reduction is due to an increase of the effective conductivity of the film and of the thermal exchange between the oil and the pads or the shaft. This is due to an increased convection in the oil. In the laminar regime, heat is conducted across the film only by diffusion through adjacent layers. Turbulent motion introduces a radial velocity term different from zero. Figure 4 shows the temperature profile across the film thickness, obtained by numerical simulations. The temperature gradient is much higher in the laminar case.

Furthermore, the use of multiple thermocouples on the pad, along the circumferential direction, showed that turbulent transition tends to also mitigate the circumferential temperature gradient [8]. In particular, while the pad maximum temperature decreases at the trailing edge, the pad minimum temperature increases at the leading edge.

In Figure 6, data from Arihara et al. are reported [46]. Both the shaft and the pad maximum temperature showed a reduction of about 10 K with an almost identical behaviour.

In Figure 6, the LTT speed is marked with a dashed line. The transition speed is approximately 70 m/s for both methods (PMT and SMT).

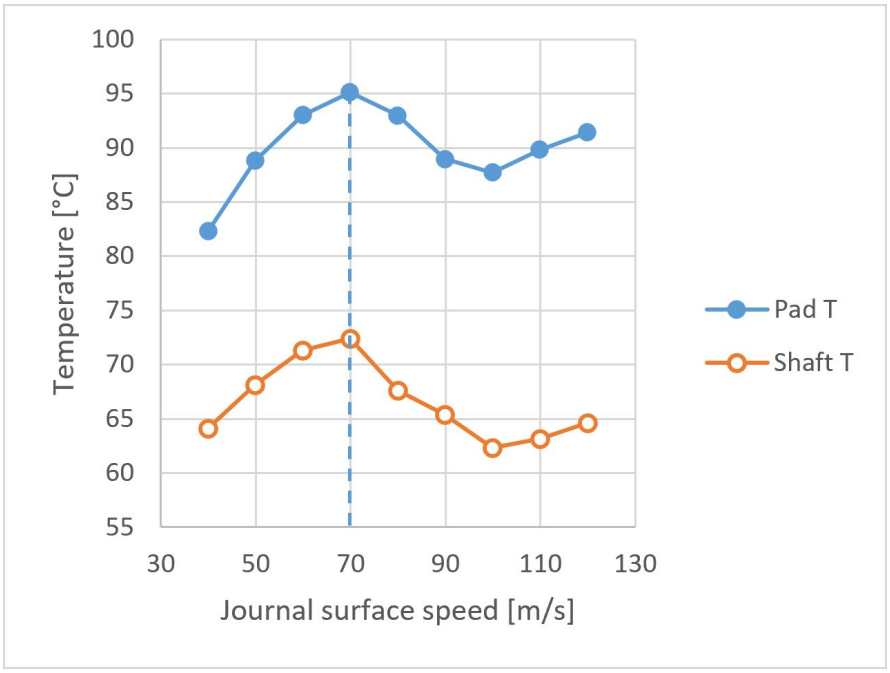

Figure 6. Pad maximum temperature and shaft temperature as a function of journal surface speed, at 2.94 MPa. The transition speed is marked with a dashed line. Data from [46].

A peculiar observation was made by Ha and Kim [70]. Their experiment was rather unique since in the laminar regime the reported pad maximum temperature was lower than the shaft temperature. The reason was not specified in the original paper—it may be due, perhaps, to an excellent thermal dissipation on the back of the pad and to a poor thermal dissipation of the shaft. In fact, at LTT, a reduction of the shaft temperature was observed at the expense of the pad temperature, which increased. The temperature reduction is visible until both the pad and the shaft reach a similar temperature (Figure 7).

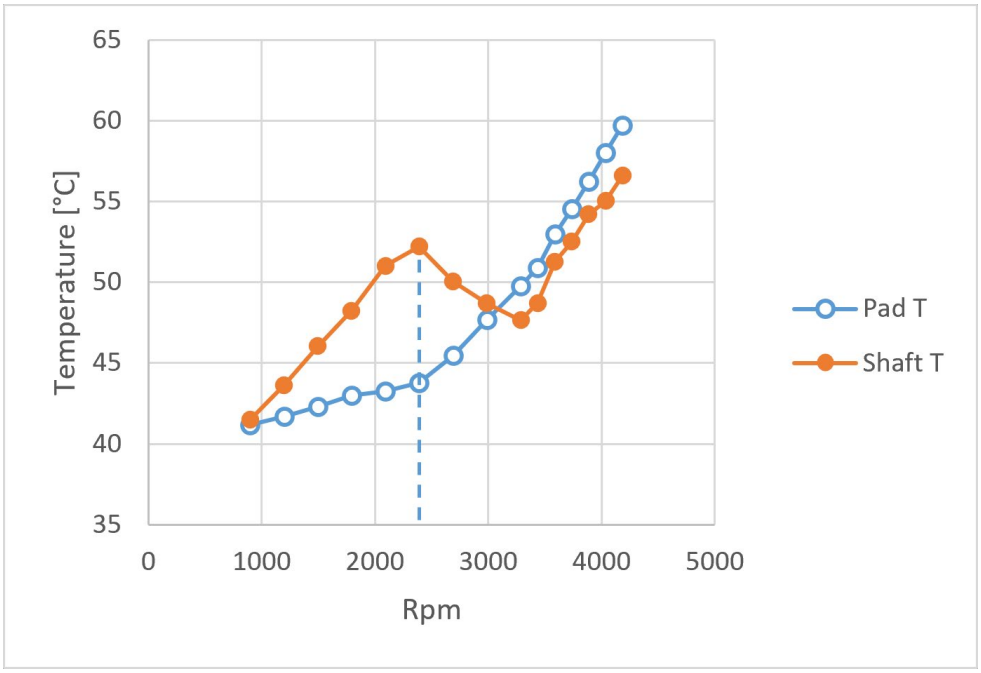

Figure 7. Pad maximum temperature and shaft temperature as functions of journal angular speed. Data from [70], with no applied load. The transition speed is marked with a dashed line.

Given that turbulence reduces thermal gradients, while the pad or the shaft reduce their maximum temperature, the lubricant increases its mean temperature [8]. As such, it turns out that monitoring the oil drain temperature can be an independent way to monitor transition (provided that the oil flow rate does not change dramatically before and after transition). Gardner [55] saw that LTT is accompanied by a sharp increase of the slope of the oil drain temperature as a function of speed. Here, this method will be abbreviated to ODT (oil discharge temperature). Unfortunately, while measurements of the oil discharge temperature are frequently made, they are rarely reported. When they are reported, there is still some uncertainty on the definition of oil drain temperature. Some authors may measure it right after the oil has exited the bearing, while others may monitor it later down the drain (see, for instance, [81]). The effect should be more evident when the thermocouple is nearest to the bearing.

Another common method of observation of the LTT is the abrupt increase of the slope of power loss as a function of speed (Figure 8). Here, this method shall be called PLI (power loss increase).

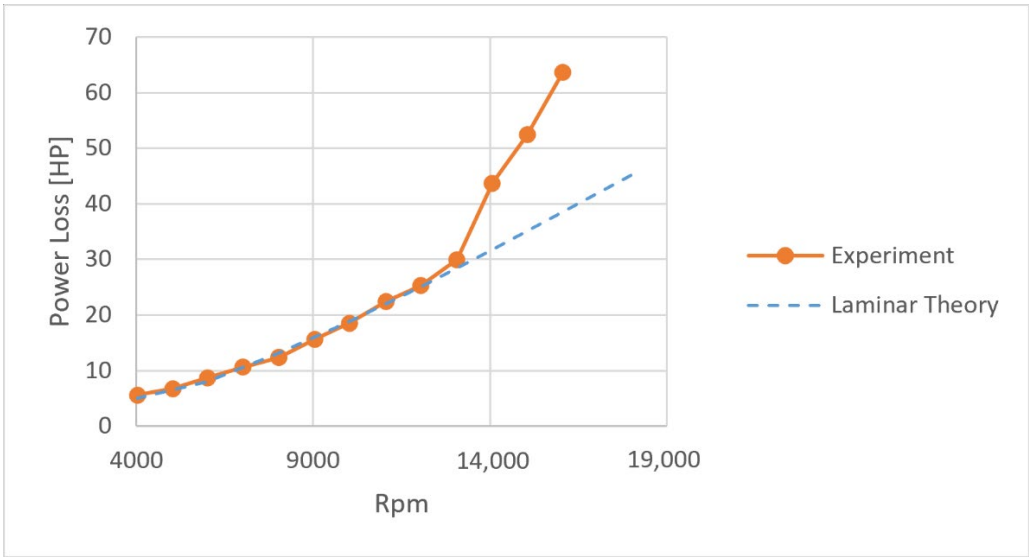

Figure 8. Power loss as a function of journal angular speed, at 0.20 MPa. Experimental points and prediction from laminar theory. Data from [71], configuration E1. Measurements were taken after a sufficiently long stabilization time.

Figure 8 reports data from Edney [71]. A sudden discontinuity in the slope of power loss is visible at about 13,000 rpm. Figure 8 also reports the results of Edney's laminar theory simulation showing that the experimental sudden increase in power loss cannot be explained through the laminar theory. This effect has been confirmed by many researchers (see Table 3) and it is detrimental to the performance of the bearing. Unfortunately, there is no easy way to get rid of this effect. It has been pointed out that using direct lubrication instead of flooded lubrication will help to decrease power loss [68]. Schüler and Berner [65] tried to keep the benefits of turbulent cooling, while limiting the unwanted PLI. Their strategy was to selectively induce turbulence in a limited region of the pad by eddy grooves.

The increase in power loss is due to the more dissipative nature of turbulent flow. From the classical theories it can be rationalized that an increase in the effective viscosity will cause an increase of power loss. It remains an open question whether the increase in eddy viscosity can be successfully countered by increasing the lubricant supply temperature above turbulent transition, and if it is convenient to do so.

Lastly, for the sake of completeness, some additional, albeit uncommon, methods to determine LTT are reported here. These observations were made by very few researchers and thus cannot be considered to be as compelling as the previously described methods.

Simmons and Dixon [69] reported turbulence by PMT. In addition, they reported a decrease of the standard deviation of the temperature at the leading edge of different pads (Figure 9).

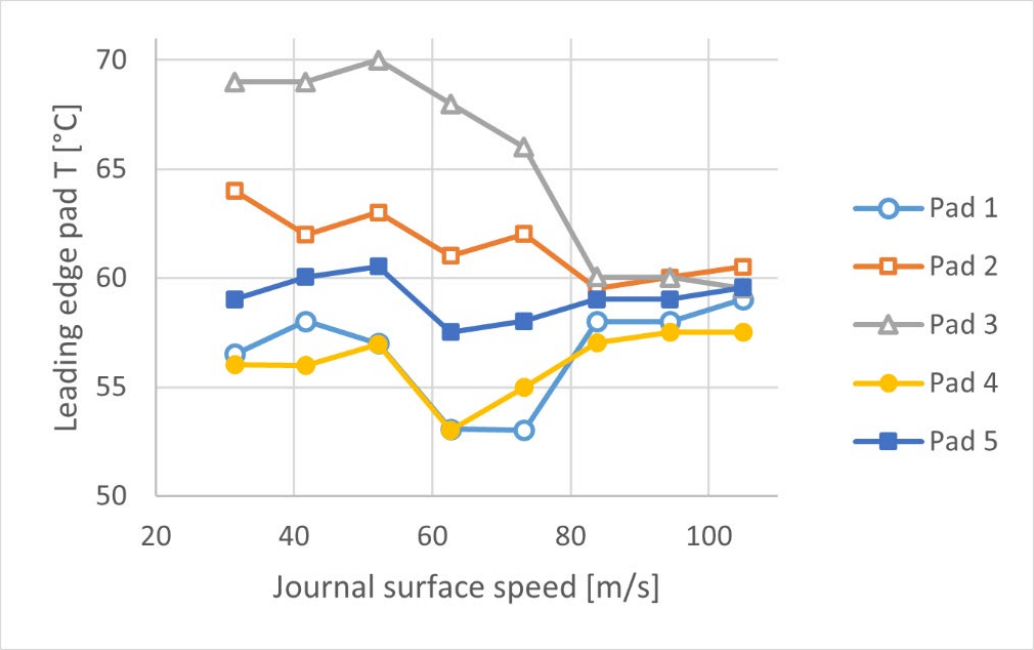

Figure 9. Leading edge pad temperature as a function of journal surface speed for a five-pad TPJB, at 2.76 MPa. The load is on pad #3. The pads are ordered following the shaft rotation. A sudden drop in the standard deviation can be seen above 80 m/s. Data from [69], configuration #1.

This is attributed, again, to the increase in thermal exchange favored by turbulence with the shaft or the housing. The hypothesis of an increased thermal exchange between consecutive pads can be discarded since the trailing edges of the pads had different temperatures. For the sake of brevity, this method is referred to as PITV (pad inlet temperature variance). In Figure 9, the transition speed according to this method is approximately 84 m/s.

Ciulli et al. [74] observed turbulence by PMT. Moreover, they reported a sudden horizontal shift in the position of the journal center, at 4000 rpm, while the bearing was vertically loaded. While this cannot be easily explained, indeed LTT might induce a sudden change in the properties of the hydrodynamic film.

Frêne [82] reported LTT by a cuspid in the graph of the mean film thickness as a function of load, at constant speed. While the experiment was on a tilting pad thrust bearing, this kind of graph may be considered by future researchers to provide additional evidence in experiments.

3.3. Effects of Parameters on Turbulent Transition

Some authors have investigated experimentally the effects of different parameters on the occurrence of turbulence such as bearing size, load, lubrication type and flow rate, and the presence of grooves.

Increasing load (that is, increasing eccentricity) tends to increase transition speed, as reported in [69,70] and as shown in Figure 5. While most authors perform experiments by sweeping the shaft speed at a constant load, in [8] LTT was observed by PMT at constant shaft speed by decreasing the load.

Contrasting results are instead reported on the effect of the oil flow rate. A decrease of the oil flow rate caused an increase of the transition speed in [71], while the opposite trend was observed in [70]. Hagemann and Schwarze [47] used several flow rates in order to

vary lubrication conditions, from fully flooded to partially starved. They reported a range of transition speeds, depending on the operating conditions, observed by PMT.

Simmons and Dixon [69] compared an LBP and an LOP configuration and observed a lower transition speed in the LBP configuration by PMT.

Edney [71] made a systematic study on the effect of various parameters on the pad temperature. The transition speed was variable depending on the configuration tested. It fell between 9000 and 13,000 rpm for the larger 127 mm bearing, and between 14,000 and 16,000 rpm for the smaller 102 mm bearing. An increase of the transition speed with lower clearances was detected, while the bearing length had no measurable influence on the transition speed.

In Ferraro et al. [73] and in Ciulli et al. [74], transition was visible in the flooded configuration at 4000 rpm, but not in the directly lubricated one. This seems to suggest that, in this case, turbulent cooling was prevalent in the secondary flow, rather than in the hydrodynamic film.

Schüler and Berner [65] compared the conventional TPJB to a grooved pad. Grooves were carved toward the trailing edge. While the grooved configurations obtained consistently lower pad temperatures across the observed speed range, no difference in power loss was found between the two configurations. They argued that turbulent flow is locally induced by the grooves, helping turbulent cooling where needed. However, in the upstream portion of the pads, the flow is still laminar. Since only a small portion of the flow is turbulent, the effect on the overall power loss is negligible. An alternative explanation is that the grooves increase the surface contact area between the fluid and the pad, thus increasing the thermal exchange between them.

3.4. Some Objections to the Evidence of Turbulent Transition in the Hydrodynamic Film

While the evidence of LTT provided by direct methods is conclusive, some researchers have speculated that the effects exploited by indirect methods may have different causes not related to turbulence. The authors agree that there is the possibility of incorrectly interpreting the results when only one of the indirect methods is used as evidence. However, if more independent methods of detecting turbulence are considered together (for instance, PMT and PLI), the possibility of getting a "false positive" is considerably reduced. Moreover, the effects ascribed to turbulence are physically justified. Any alternative explanation should also be physically justified.

Simmons and Dixon [69] assumed that turbulence in TPJBs occurs primarily in the secondary flow rather than in the hydrodynamic film. The secondary flow consists of the flow around the pads, the flow between the pads and the flow on the back of the pads. The secondary flow is a feature of TPJBs—it is not present in plain bearings. The hypothesis of Simmons and Dixon is worth investigating and could be ruled out by direct observations, which might be technologically challenging, or by probing the difference between direct and flooded lubrication.

De Choudhury and Masters [56] observed a reduction of the pad maximum temperature. They proposed an explanation alternative to turbulence with the shift of the point of maximum temperature along the pad, lowering the temperature measured by the thermocouple. This hypothesis can be ruled out by monitoring the whole pad temperature field (as, for instance, in [8]).

Stottrop et al. [68] observed a reduction of the shaft maximum temperature at about 2000 rpm in a 500 mm diameter TPJB. They tested the TPJB both in flooded and direct lubrication. The temperature drop was visible only in the DL configuration. They attributed the reduction of temperature to the onset of insufficient lubrication of the unloaded pads.

3.5. Analysis of Transitional Reynolds Number

An attempt to evaluate the Reynolds number at turbulent transition has been made for the articles reported in Table 2. The lubricant used for all tests reported was ISO VG 32 oil. Unfortunately, very few results are available regarding film thickness and viscosity

inside the meatus. For this reason, it was not possible to utilize the local Reynolds number Re_h. Therefore, the works in Table 2 were compared using the average circumferential Reynolds number Re_c defined in Equation (1). The value of viscosity of the oil is greatly affected by the oil temperature (see Equation (4)). Amongst the possible variables, it can be seen that Re_c has the greatest sensitivity to the lubricant temperature. Previous works have sometimes utilized the oil discharge temperature to calculate Re_c [55]. Unfortunately, very few authors reported the oil discharge temperature; however, most of the authors reported the oil supply temperature. The difference between the mean temperature of the film and the oil supply temperature can range from a few degrees up to 30 °C, depending on the bearing geometry, the load, the oil supply rate, and the pad and shaft temperatures. Since it may be hazardous to estimate the increase in temperature in the many different cases, the oil supply temperature was taken as a reference for Re_c. When inlet kinematic viscosity was not directly given in the papers, it was calculated using Walther's formula:

$$\log\log(\nu + 0.7) \;=\; a - b\log T \tag{4}$$

with ν in mm^2/s and T in K. The two constants (a = 9.5778, b = 3.7657) in the right-hand side were evaluated based on data available for mineral oils ISO VG 32 with Viscosity Index 100 (since no information was given about the viscosity grade of the oils employed by different authors). When more values for the terms in Equation (1) are reported in Table 2, it means that a range for the critical Reynolds number was calculated. If there is a range of possible transition speeds, the maximum was chosen.

There is a remarkable dispersion in the results. Indeed, the bearings have different features which may play a role in the experimental results. Moreover, the average Reynolds number was employed instead of the local Reynolds number. More than 80% of the values in Table 2 for the transitional Reynolds number are in the range of 250–850. The remaining values (less than 20%) are in the range of 850–1430. The majority of the values underestimate those suggested in the literature for plain bearings (1000 [4]). However, this is expected, since the oil supply temperature was considered. Since the mean temperature in the meatus is higher than the oil supply temperature, the local Reynolds number should be higher and closer to the values from the literature. It can be concluded that by calculating the Reynolds number with the oil supply temperature values, the LTT transition in a TPJB can be expected within Re_c values of 550 $\pm$ 300. However, a more precise evaluation would require the knowledge of the local Reynolds number.

4. Conclusions and Future Developments

In this work, the authors reviewed the published literature on turbulence effects in tilting pad journal bearings. The topic is vast and spans many decades. The scope of this review was limited to tilting pad journal bearings since turbulence phenomenology can be much bearing specific. Particular attention was given to recent papers not covered by previous literature reviews. After a brief introduction of the matter, numerical and experimental contributions were reviewed and extensively discussed. The main results are summarized here:

- Turbulent flow in thin films can be approximately described as laminar flow, with an effective anisotropic non-homogeneous viscosity and an effective anisotropic non-homogeneous thermal conductivity.
- Turbulent flow in TPJBs generally gives more load capacity, more power loss, higher stiffness coefficients, and higher thermal exchange between the fluid and the surfaces in contact.
- A desirable effect of turbulence is the decrease of the loaded pads highest temperature, while an undesirable one is the increase in power loss. Some of the latest research efforts aim to exploit the first while avoiding or limiting the latter.
- At present, 10^5 grid points for the hydrodynamic film are considered enough in turbulent TEHL or THL simulations, distributed mostly along the circumferential

direction or across the film thickness. This number can be reduced by one or two orders of magnitudes for turbulent HL simulations.

- In a turbulent THL simulation, if the number of points across the film thickness is much lower than 100, extra attention should be put on the convergence of the solution.
- For CFD simulations, most authors employ the RANS framework and simulate a portion of the bearing, i.e., the hydrodynamic film of a single pad, or the secondary flow between pads. Currently, one of the most used models is the SST turbulence model. In a RANS CFD simulation, 10^6 grid points are considered enough for the hydrodynamic film of a single pad.
- The field of turbulence modelling is rich and in continuous evolution. In the future, larger domains and different turbulence models are expected to be employed.
- Some numerical works compare their calculations on experimental works which are a few decades old. Future CFD and TEHL numerical researchers are suggested to consider benchmarking their calculations against more recent experimental works with, for instance, refined spatial measurement resolution of fluid film properties [66], or confidence intervals to the measurements [83].
- In most experiments reported here, LTT occurs in TPJBs at Reynolds number of 550 ± 300, provided that the Reynolds number is calculated with the oil supply temperature. More precise predictions would require knowledge of the local Reynolds number.
- Experimental works which aim to detect LTT should report as much independent evidence as possible by considering the different methods reported in this work, keeping in mind that indirect evidence is a sufficient but not a necessary condition for turbulent flow.

Finally, some future research directions are provided:

- There is a need for advanced experimental techniques to monitor velocity and temperature in ~ 10 µm thick, oil-lubricated films to provide valuable data for numerical studies, detect LTT and validate experimental indirect transition methods.
- There is a need for experiments with a denser number of rpm points in the proximity of LTT.
- The papers published in the literature should be provided with sufficient design details and material properties to allow other researchers to use them for comparison and model validation.
- The mixed lubrication performance of tilting pad journal bearings in a turbulent state may be investigated in case the bearing is heavily loaded or subjected to impact loads.

Author Contributions: Conceptualization, P.F. and E.C.; investigation, A.B. and P.F.; writing—original draft preparation, A.B.; writing—review and editing, P.F. and E.C.; visualization, A.B. and E.C.; supervision, E.C. All authors have read and agreed to the published version of the manuscript.

Funding: This research received no external funding.

Data Availability Statement: Not applicable.

Conflicts of Interest: The authors declare that they have no conflicts of interest.

Abbreviations

The following abbreviations are used in this manuscript:

B&S	Ball and socket
CFD	Computational fluid dynamics
DL	Direct lubrication
EC	Elliptical contact
FDM	Finite difference method
FEM	Finite element method
FL	Flooded lubrication
FP	Flexural pivot

FVM	Finite volume method
HL	Hydrodynamic lubrication
LBP	Load between pads
LDA	Laser doppler anemometry
LEG	Leading edge groove
LOP	Load on pads
LTT	Laminar-to-turbulent transition
ODT	Oil discharge temperature
PITV	Pad inlet temperature variance
PLI	Power loss increase
PMT	Pad maximum temperature
RANS	Reynolds-averaged Navier-Stokes
RB	Rocker back
RMS	Root mean square
SMT	Shaft maximum temperature
SST	Shear stress transport
TEG	Trailing edge groove
TEHL	Thermo-elasto-hydrodynamic lubrication
THL	Thermo-hydrodynamic lubrication
TPJB	Tilting pad journal bearing

Nomenclature

The following nomenclature is used in this manuscript:

h	Film thickness
k_x, k_y	Turbulent coefficients
p	Pressure
rpm	Rounds per minute
C	Radial clearance
D	Nominal diameter
L	Axial length
Re_h	Average circumferential Reynolds number
Re_h	Local Reynolds number
Re_{Ta}	Critical Reynolds number for Taylor vortices
Rθ	Pad arc length
U	Journal surface speed
μ	Dynamic viscosity
ν	Kinematic viscosity
Ω	Shaft angular speed

References

1. Deckler, D.C.; Veillette, R.J.; Braun, M.J.; Choy, F.K. Simulation and Control of an Active Tilting-Pad Journal Bearing. *Tribol. Trans.* **2004**, *47*, 440–458. [CrossRef]
2. Frêne, J.; Nicolas, D.; Degueurce, B.; Berthe, D.; Godet, M. *Hydrodynamic Lubrication: Bearings and Thrust Bearings*, 1st ed.; Dowson, D., Ed.; Tribol. Ser.; Elsevier: Amsterdam, The Netherlands, 1997; Volume 33, ISBN 9780444823663.
3. Lou, M.; Bareille, O.; Chai, W.; Ichchou, M.; Chen, W. Global Sensitivity Analysis of Static Characteristics of Tilting-Pad Journal Bearing to Manufacturing Tolerances. *Tribol. Int.* **2020**, *149*, 105734. [CrossRef]
4. Taylor, C.M.; Dowson, D. Turbulent Lubrication Theory—Application to Design. *J. Lubr. Technol.* **1974**, *96*, 36–46. [CrossRef]
5. Szeri, A.Z. Some Extensions of the Lubrication Theory of Osborne Reynolds. *J. Tribol.* **1987**, *109*, 21–36. [CrossRef]
6. Taylor, G. Stability of a Viscous Liquid Contained between Two Rotating Cylinders. *Philos. Trans. R. Soc. Lond.* **1923**, *223*, 289–343. [CrossRef]
7. Wilcock, D.F. Super Laminar Flow in Bearings: A Review of the Second Leeds-Lyon Symposium, Lyons, France, 17–19 September 1975. *J. Lubr. Technol.* **1976**, *98*, 5–7. [CrossRef]
8. Hopf, G.; Schüler, D. Investigations on Large Turbine Bearings Working under Transitional Conditions between Laminar and Turbulent Flow. *J. Tribol.* **1989**, *111*, 628–634. [CrossRef]
9. Mittwollen, N.; Glienicke, J. Operating Conditions of Multi-Lobe Journal Bearings Under High Thermal Loads. *J. Tribol.* **1990**, *112*, 330–338. [CrossRef]
10. Macken, N.A.; Saibel, E.A. Turbulence and Inertia Effects in Bearings. *Tribology* **1972**, *5*, 154–160. [CrossRef]

11. DiPrima, R.C.; Stuart, J.T. Non-Local Effects in the Stability of Flow between Eccentric Rotating Cylinders. *J. Fluid Mech.* **1972**, *54*, 393–415. [CrossRef]
12. Schmitt, F.G. About Boussinesq's Turbulent Viscosity Hypothesis: Historical Remarks and a Direct Evaluation of Its Validity. *Comptes Rendus Mécanique* **2007**, *335*, 617–627. [CrossRef]
13. Constantinescu, V.N. Basic Relationships in Turbulent Lubrication and Their Extension to Include Thermal Effects. *J. Lubr. Technol.* **1973**, *95*, 147–154. [CrossRef]
14. Constantinescu, V.N. On Turbulent Lubrication. *Proc. Inst. Mech. Eng.* **1959**, *173*, 881–900. [CrossRef]
15. Prandtl, L. Bericht Über Untersuchungen Zur Ausgebildeten Turbulenz. *J. Appl. Math. Mech.* **1925**, *5*, 136–139. [CrossRef]
16. Ng, C.W.; Pan, C.H.T. A Linearized Turbulent Lubrication Theory. *J. Basic Eng.* **1965**, *87*, 675–682. [CrossRef]
17. Elrod, H.G.; Ng, C.W. A Theory for Turbulent Fluid Films and Its Application to Bearings. *J. Lubr. Technol.* **1967**, *89*, 346–362. [CrossRef]
18. Hirs, G.G. A Bulk-Flow Theory for Turbulence in Lubricant Films. *J. Lubr. Technol.* **1973**, *95*, 137–145. [CrossRef]
19. Ho, M.-K.; Vohr, J.H. Application of Energy Model of Turbulence to Calculation of Lubricant Flows. *J. Lubr. Technol.* **1974**, *96*, 95–102. [CrossRef]
20. Harada, M.; Aoki, H. Analysis of Thrust Bearings Operating in Turbulent Regime. *J. Tribol.* **1988**, *110*, 555–560. [CrossRef]
21. Hashimoto, H.; Wada, S. Theoretical Approach to Turbulent Lubrication Problems Including Surface Roughness Effects. *J. Tribol.* **1989**, *111*, 17–22. [CrossRef]
22. Tieu, A.K.; Kosasih, P.B. An Expression of Reynolds Stresses in Turbulent Lubrication Theory. *J. Tribol.* **1992**, *114*, 57–60. [CrossRef]
23. Bouard, L.; Fillon, M.; Frêne, J. Comparison between Three Turbulent Models—Application to Thermohydrodynamic Performances of Tilting-Pad Journal Bearings. *Tribol. Int.* **1996**, *29*, 11–18. [CrossRef]
24. Szeri, A.Z. *Tribology: Friction, Lubrication and Wear*; McGraw-Hill: New York, NY, USA, 1980; ISBN 978-0070626638.
25. Armentrout, R.W.; He, M.; Haykin, T.; Reed, A.E. Analysis of Turbulence and Convective Inertia in a Water-Lubricated Tilting-Pad Journal Bearing Using Conventional and CFD Approaches. *Tribol. Trans.* **2017**, *60*, 1129–1147. [CrossRef]
26. Ding, A.; Ren, X.; Li, X.; Gu, C. Numerical Investigation of Turbulence Models for a Superlaminar Journal Bearing. *Adv. Tribol.* **2018**, *2018*, 2841303. [CrossRef]
27. Spalart, P.; Allmaras, S. A One-Equation Turbulence Model for Aerodynamic Flows. In Proceedings of the 30th Aerospace Sciences Meeting and Exhibit, Reno, NV, USA, 6–9 January 1992; American Institute of Aeronautics and Astronautics: Reston, VA, USA, 1992.
28. Launder, B.E.; Spalding, D.B. The Numerical Computation of Turbulent Flows. *Comput. Methods Appl. Mech. Eng.* **1974**, *3*, 269–289. [CrossRef]
29. Wilcox, D.C. Formulation of the K-w Turbulence Model Revisited. *AIAA J.* **2008**, *46*, 2823–2838. [CrossRef]
30. Menter, F.R. Two-Equation Eddy-Viscosity Turbulence Models for Engineering Applications. *AIAA J.* **1994**, *32*, 1598–1605. [CrossRef]
31. Menter, F.R. Review of the Shear-Stress Transport Turbulence Model Experience from an Industrial Perspective. *Int. J. Comput. Fluid Dyn.* **2009**, *23*, 305–316. [CrossRef]
32. Manshoor, B.; Jaat, M.; Izzuddin, Z.; Amir, K. CFD Analysis of Thin Film Lubricated Journal Bearing. *Procedia Eng.* **2013**, *68*, 56–62. [CrossRef]
33. Maneshian, B.; Nassab, S.A.G. Thermohydrodynamic Analysis of Turbulent Flow in Journal Bearings Running under Different Steady Conditions. *Proc. Inst. Mech. Eng. Part J J. Eng. Tribol.* **2009**, *223*, 1115–1127. [CrossRef]
34. Durany, J.; Pereira-Pérez, J.; Varas, F. About the Constantinescu Turbulent Model in Hydrodynamic Lubrication: A Comparison with 3-D LES Models. *Tribol. Int.* **2015**, *83*, 33–41. [CrossRef]
35. Abe, K.; Kondoh, T.; Nagano, Y. A New Turbulence Model for Predicting Fluid Flow and Heat Transfer in Separating and Reattaching Flows—I. Flow Field Calculations. *Int. J. Heat Mass Transf.* **1994**, *37*, 139–151. [CrossRef]
36. Yang, J.; Palazzolo, A. Computational Fluid Dynamics Based Mixing Prediction for Tilt Pad Journal Bearing TEHD Modeling—Part I: TEHD-CFD Model Validation and Improvements. *J. Tribol.* **2021**, *143*, 011801. [CrossRef]
37. Mermertas, Ü.; Hagemann, T.; Brichart, C. Optimization of a 900 Mm Tilting-Pad Journal Bearing in Large Steam Turbines by Advanced Modeling and Validation. *J. Eng. Gas Turbines Power* **2019**, *141*, 021033. [CrossRef]
38. Bi, C.; Han, D.; Wu, Y.; Li, Y.; Yang, J. Thermohydrodynamic Investigation for Supercritical Carbon Dioxide High Speed Tilting Pad Bearings Considering Turbulence and Real Gas Effect. *Phys. Fluids* **2021**, *33*, 125114. [CrossRef]
39. Mikami, M.; Kumagai, M.; Uno, S.; Hashimoto, H. Static and Dynamic Characteristics of Rolling-Pad Journal Bearings in Super-Laminar Flow Regime. *J. Tribol.* **1988**, *110*, 73–79. [CrossRef]
40. Orcutt, F.K. The Steady-State and Dynamic Characteristics of the Tilting-Pad Journal Bearing in Laminar and Turbulent Flow Regimes. *J. Lubr. Technol.* **1967**, *89*, 392–400. [CrossRef]
41. Okabe, E.P.; Cavalca, K.L. Rotordynamic Analysis of Systems with a Non-Linear Model of Tilting Pad Bearings Including Turbulence Effects. *Nonlinear Dyn.* **2009**, *57*, 481–495. [CrossRef]
42. Jin, Y.; Yuan, X. Analytical Method for Hydrodynamic Force in Finite-Length Tilting-Pad Journal Bearing Including Turbulence Effect. *J. Tribol.* **2020**, *142*, 091802. [CrossRef]
43. Taniguchi, S.; Makino, T.; Takeshita, K.; Ichimura, T. A Thermohydrodynamic Analysis of Large Tilting-Pad Journal Bearing in Laminar and Turbulent Flow Regimes with Mixing. *J. Tribol.* **1990**, *112*, 542–548. [CrossRef]

44. Edney, S.L.; Heitland, G.B.; DeCamillo, S.M. Testing, Analysis, and CFD Modeling of a Profiled Leading Edge Groove Tilting Pad Journal Bearing. In Proceedings of the ASME Turbo Expo, Stockholm, Sweden, 2–5 June 1998; American Society of Mechanical Engineers: New York, NY, USA, 1998; Volume 5. 98-GT-409.
45. Ikeda, K.; Hirano, T.; Yamashita, T.; Mikami, M.; Sakakida, H. An Experimental Study of Static and Dynamic Characteristics of a 580 mm (22.8 in.) Diameter Direct Lubrication Tilting Pad Journal Bearing. *J. Tribol.* **2006**, *128*, 146–154. [CrossRef]
46. Arihara, H.; Kameyama, Y.; Baba, Y.; San Andrés, L. A Thermoelastohydrodynamic Analysis for the Static Performance of High-Speed—Heavy Load Tilting-Pad Journal Bearing Operating in the Turbulent Flow Regime and Comparisons to Test Data. *J. Eng. Gas Turbines Power* **2019**, *141*, 021023. [CrossRef]
47. Hagemann, T.; Schwarze, H. Theoretical and Experimental Analyses of Directly Lubricated Tilting-Pad Journal Bearings with Leading Edge Groove. In Proceedings of the ASME Turbo Expo, Oslo, Norway, 11–15 June 2018; American Society of Mechanical Engineers: New York, NY, USA, 2018; Volume 7B-2018. GT2018-75659.
48. Hagemann, T.; Zemella, P.; Pfau, B.; Schwarze, H. Experimental and Theoretical Investigations on Transition of Lubrication Conditions for a Five-Pad Tilting-Pad Journal Bearing with Eccentric Pivot up to Highest Surface Speeds. *Tribol. Int.* **2020**, *142*, 106008. [CrossRef]
49. Buchhorn, N.; Stottrop, M.; Bender, B. Influence of Active Cooling at the Trailing Edge on the Thermal Behavior of a Tilting-Pad Journal Bearing. *Lubricants* **2021**, *9*, 26. [CrossRef]
50. Bouard, L.; Fillon, M.; Frêne, J. Thermohydrodynamic Analysis of Tilting-Pad Journal Bearings Operating in Turbulent Flow Regime. *J. Tribol.* **1996**, *118*, 225–231. [CrossRef]
51. Tanaka, M.; Hatakenaka, K. Turbulent Thermohydrodynamic Lubrication Models Compared with Measurements. *Proc. Inst. Mech. Eng. Part J J. Eng. Tribol.* **2004**, *218*, 391–399. [CrossRef]
52. Hatakenaka, K. A New Turbulent Thermohydrodynamic Performance Analysis of Tilting Pad Journal Bearing Based on a K-ε Model and Comparison with Measurements. *Trans. JSME* **2015**, *81*, 15-00253. (In Japanese) [CrossRef]
53. Hagemann, T.; Zeh, C.; Prölß, M.; Schwarze, H. The Impact of Convective Fluid Inertia Forces on Operation of Tilting-Pad Journal Bearings. *Int. J. Rotating Mach.* **2017**, *2017*, 5683763. [CrossRef]
54. Ettles, C.M. The Analysis of Pivoted Pad Journal Bearing Assemblies Considering Thermoelastic Deformation and Heat Transfer Effects. *Tribol. Trans.* **1992**, *35*, 156–162. [CrossRef]
55. Gardner, W.W.; Ulschmid, J.G. Turbulence Effects in Two Journal Bearing Applications. *J. Lubr. Technol.* **1974**, *96*, 15–20. [CrossRef]
56. De Choudhury, P.; Masters, D.A. Performance Tests of Five-Shoe Tilting-Pad Journal Bearing. *ASLE Trans.* **1984**, *27*, 61–66. [CrossRef]
57. Brockwell, K.R.; Kleinbub, D. Measurements of the Steady State Operating Characteristics of the Five Shoe Tilting Pad Journal Bearing. *Tribol. Trans.* **1989**, *32*, 267–275. [CrossRef]
58. Croné, P.; Almqvist, A.; Larsson, R. Thermal Turbulent Flow in Leading Edge Grooved and Conventional Tilting Pad Journal Bearing Segments—A Comparative Study. *Lubricants* **2018**, *6*, 97. [CrossRef]
59. Fillon, M.; Desbordes, H.; Frêne, J.; Chan Hew Wai, C. A Global Approach of Thermal Effects Including Pad Deformations in Tilting-Pad Journal Bearings Submitted to Unbalance Load. *J. Tribol.* **1996**, *118*, 169–174. [CrossRef]
60. Carter, C.R. Measured and Predicted Rotordynamic Coefficients and Static Performance of a Rocker-Pivot Tilt Pad Bearing in Load-on-Pad and Load-between-Pad Configurations. M.S. Thesis, Texas A&M University, College Station, TX, USA, 2007.
61. Kulhanek, C.D. Dynamic and Static Characteristics of a Rocker-Pivot, Tilting-Pad Bearing with 50% and 60% Offsets. M.S. Thesis, Texas A&M University, College Station, TX, USA, 2010.
62. Someya, T.; Mitsui, J.; Esaki, J.; Saito, S.; Kanemitsu, Y.; Iwatsubo, T.; Tanaka, M.; Hisa, S.; Fujikawa, T.; Kanki, H. *Journal-Bearing Databook*; Springer Science & Business Media: Berlin, Germany, 2013.
63. Yang, J.; Palazzolo, A. Three-Dimensional Thermo-Elasto-Hydrodynamic Computational Fluid Dynamics Model of a Tilting Pad Journal Bearing—Part I: Static Response. *J. Tribol.* **2019**, *141*, 061702. [CrossRef]
64. Zemella, P.; Hagemann, T.; Pfau, B.; Schwarze, H. Identification of Dynamic Coefficients of a Five-Pad Tilting Pad Journal Bearing up to Highest Surface Speeds. *J. Eng. Gas Turbines Power.* **2021**, *143*, 081013. [CrossRef]
65. Schüler, E.; Berner, O. Improvement of Tilting-Pad Journal Bearing Operating Characteristics by Application of Eddy Grooves. *Lubricants* **2021**, *9*, 18. [CrossRef]
66. Hagemann, T.; Kukla, S.; Schwarze, H. Measurement and Prediction of the Static Operating Conditions of a Large Turbine Tilting-Pad Bearing under High Circumferential Speeds and Heavy Loads. In Proceedings of the ASME Turbo Expo, San Antonio, TX, USA, 3–7 June 2013; American Society of Mechanical Engineers: New York, NY, USA, 2013; Volume 7 B. GT2013-95004.
67. Kukla, S.; Hagemann, T.; Schwarze, H. Measurement and Prediction of the Dynamic Characteristics of a Large Turbine Tilting-Pad Bearing under High Circumferential Speeds. In Proceedings of the ASME Turbo Expo, San Antonio, TX, USA, 3–7 June 2013; American Society of Mechanical Engineers: New York, NY, USA, 2013; Volume 7 B. GT2013-95074.
68. Stottrop, M.; Buchhorn, N.; Bender, B. Experimental Investigation of a Large Tilting-Pad Journal Bearing—Comparison of a Flooded and Non-Flooded Design. *Lubricants* **2022**, *10*, 83. [CrossRef]
69. Simmons, J.E.L.; Dixon, S.J. Effect of Load Direction, Preload, Clearance Ratio, and Oil Flow on the Performance of a 200mm Journal Pad Bearing. *Tribol. Trans.* **1994**, *37*, 227–236. [CrossRef]

70. Ha, H.C.; Kim, H.J.; Kim, K.W. Inlet Pressure Effects on the Thermohydrodynamic Performance of a Large Tilting Pad Journal Bearing. *J. Tribol.* **1995**, *117*, 160–165. [CrossRef]
71. Edney, S. Pad Temperature in High Speed, Lightly Loaded Tilting Pad Journal Bearings. In Proceedings of the 24th Turbomachinery Symposium, Houston, TX, USA, 26 September 1995; pp. 73–84.
72. Bouchoule, C.; Fillon, M.; Nicolas, D.; Barresi, F. Experimental Study of Thermal Effects in Tilting-Pad Journal Bearings at High Operating Speeds. *J. Tribol.* **1996**, *118*, 532–538. [CrossRef]
73. Ferraro, R.; Innocenti, A.; Libraschi, M.; Barsanti, M.; Ciulli, E.; Forte, P.; Nuti, M. Dynamic Identification of 280mm Diameter Tilting Pad Journal Bearings: Test Results and Measurement Uncertainties Assessment of Different Designs. In Proceedings of the ASME Turbo Expo, Virtual, Online, 21–25 September 2020; American Society of Mechanical Engineers: New York, NY, USA, 2020; Volume 10A-2020. GT2020-14718.
74. Ciulli, E.; Ferraro, R.; Forte, P.; Innocenti, A.; Nuti, M. Experimental Characterization of Large Turbomachinery Tilting Pad Journal Bearings. *Machines* **2021**, *9*, 273. [CrossRef]
75. Frêne, J.; Godet, M. Flow Transition Criteria in a Journal Bearing. *J. Tribol.* **1974**, *96*, 135–140. [CrossRef]
76. Innes, G.E.; Leutheusser, H.J. An Investigation into Laminar-to-Turbulent Transition in Tilting-Pad Bearings. *J. Tribol.* **1991**, *113*, 303–307. [CrossRef]
77. Tieu, A.K.; Kosasih, P.B.; Mackenzie, M.R. A Study of Fluid Velocities in Tribological Fluid Film. *J. Tribol.* **1994**, *116*, 133–138. [CrossRef]
78. Nobis, M.; Reinke, P.; Schmidt, M.; Riedel, M.; Redlich, M. Investigation of the Velocity Distribution in the Flow of a Journal Bearing Model. *EPJ Web Conf.* **2014**, *67*, 02083. [CrossRef]
79. Tropea, C. Laser Doppler Anemometry: Recent Developments and Future Challenges. *Meas. Sci. Technol.* **1995**, *6*, 605–619. [CrossRef]
80. American Petroleum Institute. *Machinery Protection Systems*, 5th ed.; American Petroleum Institute: Washington, DC, USA, 2014.
81. De Choudhury, P.; Barth, E.W. A Comparison of Film Temperatures and Oil Discharge Temperature for a Tilting-Pad Journal Bearing. *J. Lubr. Technol.* **1981**, *103*, 115–119. [CrossRef]
82. Frêne, J. Tapered Land Thrust Bearing Operating in Both Laminar and Turbulent Regimes. *ASLE Trans.* **1978**, *21*, 243–249. [CrossRef]
83. Barsanti, M.; Ciulli, E.; Forte, P. Random Error Propagation and Uncertainty Analysis in the Dynamic Characterization of Tilting Pad Journal Bearings. *J. Phys. Conf. Ser.* **2019**, *1264*, 012035. [CrossRef]